Piippo, Antti; Hinkkanen, Marko; Luomi, Jorma

Adaptation of motor parameters in sensorless PMSM drives

Published in:
IEEE Transactions on Industry Applications

DOI:
10.1109/TIA.2008.2009614

Published: 20/01/2009

Document Version
Peer reviewed version

Please cite the original version:
Piippo, A., Hinkkanen, M., & Luomi, J. (2009). Adaptation of motor parameters in sensorless PMSM drives. *IEEE Transactions on Industry Applications*, *45*(1), 203-212. https://doi.org/10.1109/TIA.2008.2009614

Adaptation of Motor Parameters in Sensorless PMSM Drives

Antti Piippo, Marko Hinkkanen, *Member, IEEE,* and Jorma Luomi *Member, IEEE*

***Abstract*—The paper proposes an on-line method for the estimation of the stator resistance and the permanent magnet flux in sensorless permanent magnet synchronous motor drives. An adaptive observer augmented with a high-frequency signal injection technique is used for sensorless control. The observer contains excess information that is not used for the speed and position estimation. This information is used for the adaptation of the motor parameters: at low speeds, the stator resistance is estimated, whereas at medium and high speeds, the permanent magnet flux is estimated. Small-signal analysis is carried out to investigate the proposed method. The convergence of the parameter estimates is shown by simulations and laboratory experiments. The stator resistance adaptation works down to zero speed in sensorless control.**

***Index Terms*—Permanent magnet motors, Parameter adaptation, Sensorless control, Signal injection.**

I. Introduction

Permanent magnet synchronous machines (PMSMs) are used in many high-performance applications. For vector control of PMSMs, information on the rotor position is required. In sensorless control, the methods for estimating the rotor speed and position can be classified into two categories: fundamental-excitation methods [1], [2] and signal injection methods [3], [4]. The methods can also be combined by changing the estimation method as the rotor speed varies [5], [6].

The fundamental-excitation methods used for sensorless control are based on models of the PMSM. Hence, the electrical parameters are needed for the speed and position estimation [7]. The errors in the stator resistance estimate result in an incorrect back-emf estimate and, consequently, impaired position estimation accuracy. The operation can also become unstable at low speeds in a loaded condition. The detuned estimate of the permanent magnet (PM) flux results in incorrectly estimated electromagnetic torque [8], and also impairs the position estimation accuracy. Errors in the d- and q-axis inductances of a salient PMSM also affect the estimation and the torque production, and can degrade the current control performance.

The stator resistance and the PM flux depend on the motor temperature, and thus change rather slowly. On the other hand, magnetic saturation decreases the inductances, which thus depend on the load condition. The inductances can be modeled as functions of the stator flux or the stator current, but an estimation scheme is required for the stator resistance and the PM flux. The back-emf is proportional to the PM flux and the resistive voltage drop to the stator resistance. At medium and high speeds, the effect of the PM flux estimation error is more significant than that of the stator resistance estimation error. On the other hand, the back-emf is small at low speeds, and the stator resistance estimate plays an important role in the estimation.

Several methods have been proposed to improve the performance of a PMSM drive by estimating the electrical parameters. In [7], an MRAS scheme is used for the on-line estimation of the stator resistance and the PM flux with position measurement. Reactive power feedback is used for estimating the PM flux in [9], and the PM flux is estimated by taking it as an additional state of an extended Kalman filter in [10]. The stator current estimation error and a neural network can be used for estimating both the PM flux and the stator resistance [11]. The stator inductances and the PM flux are estimated using the steady-state voltage equations and the flux harmonics, respectively, in [12]. A dc-current signal is injected to detect the resistive voltage drop for the resistance estimation in [13]. It has been proposed that the total resistance and temperature of an induction motor can be estimated from the small-signal impedance using high-frequency signal injection [14].

Some parameter estimation schemes have also been developed for sensorless control methods. In [7], an MRAS scheme is applied for the stator resistance estimation. A parameter estimator is added to two position estimation methods for estimating the stator resistance and the PM flux in [15]. In [16], these parameters are estimated using both the steady-state motor equations and the response to an alternating current signal. In [15], [16], the convergence of the estimated parameters to their actual values is not shown. [17] proposes a method where the resistance and the inductances of a salient PMSM are extracted from an extended EMF model. Three electrical parameters are estimated simultaneously, but the behavior of the stator resistance estimate is not convincing.

The parameters of the PMSM are needed in fundamental-excitation methods, but signal injection methods are not sensitive to the parameter errors. If a combination of these two method types is used for speed and position estimation, the signal injection is usually removed as the speed increases, and the sensitivity to the parameter errors increases. Therefore, combined methods need the parameter estimates with sufficient accuracy although signal injection is used at low speeds.

This work was financially supported by ABB Oy, Walter Ahlström foundation, and KAUTE foundation.

Antti Piippo is with ABB Oy, Drives, P.O. Box 184, FI-00381 Helsinki, Finland (e-mail: antti.piippo@fi.abb.com). Marko Hinkkanen and Jorma Luomi are with Helsinki University of Technology, Department of Electrical Engineering, P.O. Box 3000, FI-02015 TKK, Finland.

This paper proposes a method for the on-line estimation of the stator resistance and the PM flux in sensorless control. The method is based on a speed-adaptive observer that is augmented with a high-frequency (HF) signal injection technique at low speeds [18]. The excess information available in the observer is used for the adaptation of the parameters. At medium and high speeds, the PM flux is estimated from the d-axis current estimation error. At low speeds, the stator resistance is estimated from an error signal produced by the signal injection method. The stability and the convergence of the parameter estimators are investigated by means of small-signal analysis, simulations, and laboratory experiments. The resistance adaptation is shown to work down to zero speed in sensorless control.

II. PMSM Model

The PMSM is modeled in the d-q reference frame fixed to the rotor. The d axis is oriented along the PM flux, whose angle in the stator reference frame is θ_m in electrical radians. The stator voltage equation is

$$\mathbf{u}_s = R_s\mathbf{i}_s + \dot{\boldsymbol{\psi}}_s + \omega_m\mathbf{J}\boldsymbol{\psi}_s \tag{1}$$

where $\mathbf{u}_s = [\,u_d \;\; u_q\,]^T$ is the stator voltage, $\mathbf{i}_s = [\,i_d \;\; i_q\,]^T$ the stator current, $\boldsymbol{\psi}_s = [\,\psi_d \;\; \psi_q\,]^T$ the stator flux, R_s the stator resistance, $\omega_m = \dot{\theta}_m$ the electrical angular speed of the rotor, and

$$\mathbf{J} = \begin{bmatrix} 0 & -1 \\ 1 & 0 \end{bmatrix}$$

The stator flux is

$$\boldsymbol{\psi}_s = \mathbf{L}\mathbf{i}_s + \boldsymbol{\psi}_{pm} \tag{2}$$

where $\boldsymbol{\psi}_{pm} = [\,\psi_{pm} \;\; 0\,]^T$ is the PM flux and

$$\mathbf{L} = \begin{bmatrix} L_d & 0 \\ 0 & L_q \end{bmatrix}$$

is the inductance matrix, L_d and L_q being the direct- and quadrature-axis inductances, respectively. The electromagnetic torque is given by

$$T_e = \frac{3p}{2}\boldsymbol{\psi}_s^T\mathbf{J}^T\mathbf{i}_s \tag{3}$$

where p is the number of pole pairs.

III. Speed and Position Estimation

A. Control System

Fig. 1 shows the block diagram of the control system comprising cascaded speed and current control loops. PI-type speed control with active damping is used. The adaptive observer provides the speed and position estimates $\hat{\omega}_m$ and $\hat{\theta}_m$, respectively. The motor parameters are needed in the adaptive observer, in the current controller, and in the calculation of the stator current component references according to the maximum torque-per-ampere method [19].

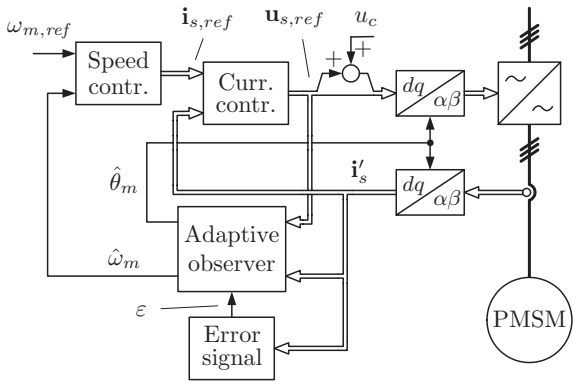

Fig. 1. Block diagram of the control system. Error signal ε is evaluated based on HF signal injection. Block "Speed contr." includes both the speed controller and the minimization of the current amplitude.

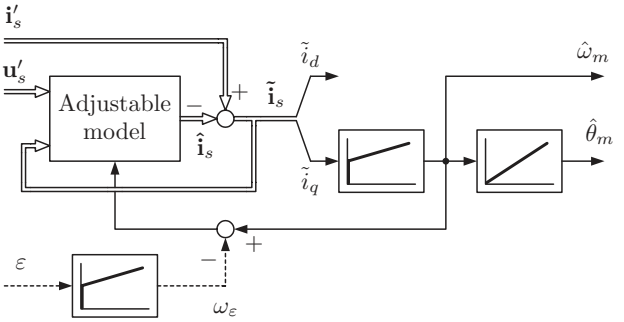

Fig. 2. Block diagram of the adaptive observer without parameter adaptation. Signals ε and ω_ε, obtained from the HF signal injection method, are used only at low speeds.

B. Adaptive Observer

The adaptive observer shown in Fig. 2 is used for the estimation of the rotor speed and rotor position [18]. The speed and position estimation is based on the estimation error between two different models; the actual motor can be considered as a reference model and the observer—including the rotor speed estimate $\hat{\omega}_m$—as an adjustable model. The speed adaptation is based on the estimation error of the stator current. The estimated rotor speed is fed back to the adjustable model.

The adaptive observer is formulated in the estimated rotor reference frame. The adjustable model is based on (1) and (2), and defined by

$$\dot{\hat{\boldsymbol{\psi}}}_s = \mathbf{u}'_s - \hat{R}_s\hat{\mathbf{i}}_s - \hat{\omega}_m\mathbf{J}\hat{\boldsymbol{\psi}}_s + \boldsymbol{\lambda}\tilde{\mathbf{i}}_s \tag{4}$$

where $\mathbf{u}'_s$ is the stator voltage in the estimated rotor reference frame, $\boldsymbol{\lambda}$ is the observer gain matrix, and estimated quantities are marked by $\hat{}$. The estimate of the stator current and the estimation error of the stator current are

$$\hat{\mathbf{i}}_s = \mathbf{L}^{-1}(\hat{\boldsymbol{\psi}}_s - \hat{\boldsymbol{\psi}}_{pm}) \tag{5}$$

$$\tilde{\mathbf{i}}_s = \mathbf{i}'_s - \hat{\mathbf{i}}_s \tag{6}$$

respectively, where $\mathbf{i}'_s$ is the measured stator current expressed in the estimated rotor reference frame and $\hat{\boldsymbol{\psi}}_{pm} = [\,\hat{\psi}_{pm} \;\; 0\,]^T$. The observer gain matrix $\boldsymbol{\lambda}$ depends on the estimated rotor

speed [18],

$$\boldsymbol{\lambda} = \begin{cases} 2\hat{R}_s \left[\frac{|\hat{\omega}_m|}{\omega_B}\mathbf{I} + \frac{\hat{\omega}_m}{\omega_B}\mathbf{J} \right], & |\hat{\omega}_m| \leq \omega_B \\ 2\hat{R}_s \left[\mathbf{I} + \mathrm{sign}(\hat{\omega}_m)\mathbf{J} \right], & |\hat{\omega}_m| > \omega_B \end{cases} \tag{7}$$

where ω_B is the base value of the angular frequency.

The speed adaptation is based on the current estimation error in the estimated q direction. The estimate of the electrical angular speed of the rotor is obtained using a PI speed adaptation mechanism

$$\hat{\omega}_m = -\mathbf{k}_p \tilde{\mathbf{i}}_s - \mathbf{k}_i \int \tilde{\mathbf{i}}_s dt \tag{8}$$

where $\mathbf{k}_p = [0 \;\; k_p]$ and $\mathbf{k}_i = [0 \;\; k_i]$. The nonnegative gains k_p and k_i are selected as [20]

$$k_p = \frac{2\alpha_{fo}}{\hat{\psi}_{pm}/L_q}, \quad k_i = \frac{\alpha_{fo}^2}{\hat{\psi}_{pm}/L_q} \tag{9}$$

where α_{fo} is the design parameter. The parameter α_{fo} can be interpreted as an approximate speed-adaptation bandwidth, and it determines the tracking errors in transients. The rotor position estimate is

$$\hat{\theta}_m = \int \hat{\omega}_m dt \tag{10}$$

C. Combined Observer

At low speeds, the adaptive observer described above is augmented with an HF signal injection method to stabilize the speed and position estimation [18]. An alternating voltage was selected for HF signal injection. A carrier excitation signal varying sinusoidally at angular frequency ω_c and having amplitude $\hat{u}_c$, i.e.

$$u_c = \hat{u}_c \cos(\omega_c t) \tag{11}$$

is superimposed on the d component of the stator voltage in the estimated rotor reference frame. An alternating HF current response is detected in the q direction of the estimated rotor reference frame, amplitude modulated by the rotor position estimation error. The q component of the measured current is band-pass filtered (BPF), giving an HF current signal i_{qc} that varies at the signal injection frequency. The current signal is then demodulated and low-pass filtered (LPF) to extract an error signal

$$\varepsilon = \mathrm{LPF}\{i_{qc} \sin(\omega_c t)\} \tag{12}$$

Ideally, this error signal is

$$\varepsilon = \underbrace{\frac{\hat{u}_c}{\omega_c} \frac{L_q - L_d}{4L_q L_d}}_{K_\varepsilon} \sin(2\tilde{\theta}_m) \tag{13}$$

where K_ε can be considered as the signal injection gain and $\tilde{\theta}_m = \theta_m - \hat{\theta}_m$ is the estimation error of the rotor position.

For the combined observer, the adjustable model (4) is modified to

$$\dot{\hat{\boldsymbol{\psi}}}_s = \mathbf{u}_s' - \hat{R}_s \hat{\mathbf{i}}_s - (\hat{\omega}_m - \omega_\varepsilon)\mathbf{J}\hat{\boldsymbol{\psi}}_s + \boldsymbol{\lambda}\tilde{\mathbf{i}}_s \tag{14}$$

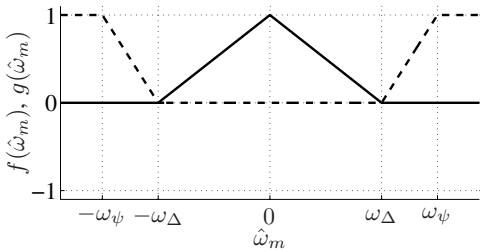

Fig. 3. Functions $f(\hat{\omega}_m)$ (solid) and $g(\hat{\omega}_m)$ (dashed) as functions of estimated rotor speed.

where the signal

$$\omega_\varepsilon = \gamma_p \varepsilon + \gamma_i \int \varepsilon dt \tag{15}$$

corrects the angular speed of the stator flux estimate. The PI mechanism, having the gains γ_p and γ_i, drives the error signal ε to zero. Other parts of the adaptive observer are not modified, i.e. (5)–(10) hold for the combined observer. The gains in (15) are selected as [6]

$$\gamma_p = \frac{\alpha_i}{2K_\varepsilon}, \quad \gamma_i = \frac{\alpha_i^2}{6K_\varepsilon} \tag{16}$$

where α_i is the approximate bandwidth of the PI mechanism (15), assuming the speed adaptation (8) is much faster than the PI mechanism (15).

As can be seen in Fig. 2, the signal ω_ε corrects the position estimate indirectly through the speed adaptation mechanism (8). The signal injection method dominates in steady state, whereas the adaptive observer commands at transients. It is to be noted that the factor $(\hat{\omega}_m - \omega_\varepsilon)$ in (14) differs from the estimated speed $\hat{\omega}_m$ used for the speed control and for the position estimation. The signal ω_ε compensates for the parameter errors in the adjustable model and for errors in the measurements.

At low speeds, the combined observer relies both on the signal injection method and on the adaptive observer. The effect of the signal injection method is reduced linearly as the rotor speed increases, reaching zero at the transition speed ω_Δ. Both the HF excitation voltage $\hat{u}_c$ and the approximate bandwidth α_i of the PI mechanism in (15) are decreased, i.e.

$$\hat{u}_c = f(\hat{\omega}_m)\hat{u}_c', \quad \alpha_i = f(\hat{\omega}_m)\alpha_i' \tag{17}$$

where $\hat{u}_c'$ and α_i' are the zero-speed values of the HF excitation voltage and the PI mechanism bandwidth, respectively. The function $f(\hat{\omega}_m)$ is shown in Fig. 3. At speeds higher than the transition speed ω_Δ, the HF signal injection is not used.

IV. Parameter Adaptation

A. Proposed Adaptation Laws

At most two parameters can be estimated simultaneously in steady state if only fundamental excitation is used. The component $\tilde{i}_q$ of the current estimation error is used for the speed estimation in this paper, while the PM flux is adjusted using $\tilde{i}_d$ according to

$$\hat{\psi}_{pm} = -\mathbf{k}_\psi \int \tilde{\mathbf{i}}_s dt \tag{18}$$

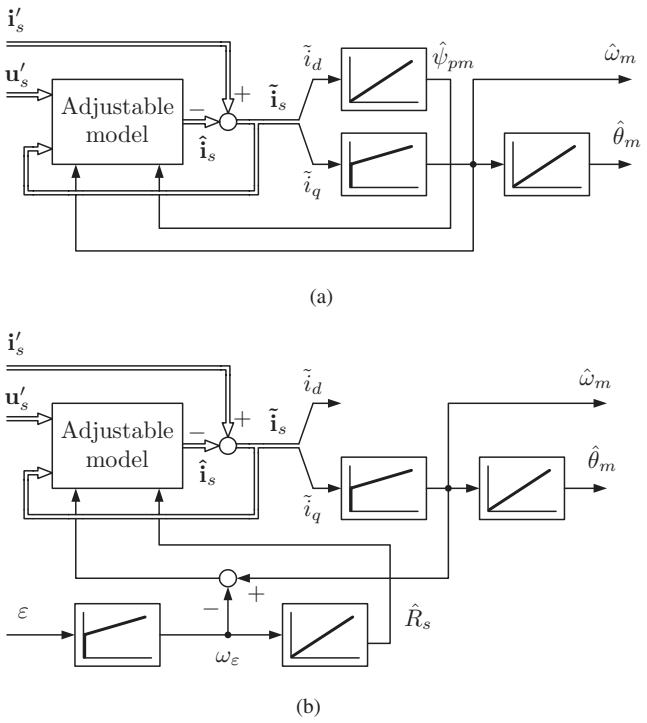

Fig. 4. Block diagram of the adaptive observer with parameter adaptation: (a) PM flux adaptation at medium and high speeds ($|\hat{\omega}_m| \geq \omega_\Delta$); (b) stator resistance adaptation at low speeds ($|\hat{\omega}_m| < \omega_\Delta$).

where $\mathbf{k}_\psi = [k_\psi \;\; 0]$ and k_ψ is the nonnegative adaptation gain. Since the effect of the PM flux error on the current estimation error $\tilde{\mathbf{i}}_s$ is decreased at low speeds, the adaptation law (18) is enabled only at medium and high speeds. The observer including the PM flux adaptation is shown in Fig. 4(a), where the adjustable model is based on (4) and (5).

At low speeds, the effect of the stator resistance error on the current estimation error $\tilde{\mathbf{i}}_s$ is much larger than the effect of the PM flux error. Hence, it would be reasonable to estimate the stator resistance from $\tilde{\mathbf{i}}_s$ (in addition to the rotor speed). Designing a simultaneous estimation method for the stator resistance (or the PM flux) and the rotor speed at low speeds, using only fundamental excitation, is a very challenging task.[1] However, the HF signal injection method provides information through the signal ω_ε. If ω_ε differs from zero in steady state at low speeds, motor parameter estimates are inaccurate. Hence, the stator resistance is estimated at low speeds by integration from ω_ε as

$$\hat{R}_s = -k_R \int \omega_\varepsilon dt \tag{19}$$

where k_R is the adaptation gain. The observer, including the PI mechanism (15) of the HF signal injection and the adaptation mechanism (19), is shown in Fig. 4(b), where the adjustable model is based on (5) and (14).

In order to analyze the parameter adaptation loops more thoroughly, a linearized open-loop model for current estimation error dynamics is derived in Section IV-B. The tuning of the adaptation gains is considered in Section IV-C based on the linearized model in quasi-steady state. Then, the local stability of the closed-loop system is analyzed in Section IV-D.

[1]For induction motors, some interesting approaches have been proposed [21], [22].

B. Open-Loop Dynamics of Estimation Error

Based on the motor model (1) expressed in the estimated rotor reference frame and the observer (14), the open-loop dynamics of the current estimation error are

$$\dot{\tilde{\boldsymbol{\psi}}}_s = -(R_s\mathbf{I} + \boldsymbol{\lambda})\tilde{\mathbf{i}}_s - \hat{\omega}_m\mathbf{J}\tilde{\boldsymbol{\psi}}_s - \tilde{R}_s\hat{\mathbf{i}}_s - \omega_\varepsilon\mathbf{J}\hat{\boldsymbol{\psi}}_s \tag{20a}$$

$$\begin{aligned}\tilde{\mathbf{i}}_s = {} & e^{\mathbf{J}\tilde{\theta}_m}\mathbf{L}^{-1}e^{-\mathbf{J}\tilde{\theta}_m}(\tilde{\boldsymbol{\psi}}_s - \tilde{\boldsymbol{\psi}}_{pm}) \\ & + \left(e^{\mathbf{J}\tilde{\theta}_m}\mathbf{L}^{-1}e^{-\mathbf{J}\tilde{\theta}_m} - \mathbf{L}^{-1}\right)(\hat{\boldsymbol{\psi}}_s - \hat{\boldsymbol{\psi}}_{pm})\end{aligned} \tag{20b}$$

The estimation error of the PM flux vector is

$$\tilde{\boldsymbol{\psi}}_{pm} = \boldsymbol{\psi}'_{pm} - \hat{\boldsymbol{\psi}}_{pm} = \left(e^{\mathbf{J}\tilde{\theta}_m} - \mathbf{I}\right)\boldsymbol{\psi}_{pm} + \begin{bmatrix}\tilde{\psi}_{pm}\\ 0\end{bmatrix} \tag{21}$$

where $\boldsymbol{\psi}'_{pm} = e^{\mathbf{J}\tilde{\theta}_m}\boldsymbol{\psi}_{pm}$ is the actual PM flux vector in the estimated coordinates. The system (20) can be linearized about the steady-state operating point:

$$\dot{\tilde{\boldsymbol{\psi}}}_s = -(R_s\mathbf{I} + \boldsymbol{\lambda}_0)\tilde{\mathbf{i}}_s - \omega_{m0}\mathbf{J}\tilde{\boldsymbol{\psi}}_s - \mathbf{i}_{s0}\tilde{R}_s - \mathbf{J}\boldsymbol{\psi}_{s0}\omega_\varepsilon \tag{22a}$$

$$\tilde{\mathbf{i}}_s = \mathbf{L}^{-1}\tilde{\boldsymbol{\psi}}_s - \mathbf{L}^{-1}(\mathbf{J}\boldsymbol{\psi}_{s0} - \mathbf{L}\mathbf{J}\mathbf{i}_{s0})\,\tilde{\theta}_m - \mathbf{L}^{-1}\begin{bmatrix}\tilde{\psi}_{pm}\\ 0\end{bmatrix} \tag{22b}$$

where operating-point quantities are marked with the subscript 0 and the operating-point estimation errors are assumed to be zero. The current estimation error $\tilde{\mathbf{i}}_s$ can be considered as the output of the system while $\tilde{\theta}_m$, $\tilde{\psi}_{pm}$, $\tilde{R}_s$, and ω_ε are the inputs. After substituting the output equation (22b) for $\tilde{\mathbf{i}}_s$ in (22a), the system can be expressed in the standard state-space form, as shown in (37) in the Appendix.

C. Quasi-Steady-State Analysis

Here, the estimation error dynamics (22) are considered to be much faster than the parameter adaptation mechanisms. Because of the different time scales, the system (22) can be considered from the viewpoint of parameter adaptation in steady state:

$$\begin{aligned}\omega_{m0}\mathbf{J}\left\{\mathbf{L}\tilde{\mathbf{i}}_s + (\mathbf{J}\boldsymbol{\psi}_{s0} - \mathbf{L}\mathbf{J}\mathbf{i}_{s0})\,\tilde{\theta}_m + \begin{bmatrix}\tilde{\psi}_{pm}\\ 0\end{bmatrix}\right\} \\ = -(R_s\mathbf{I} + \boldsymbol{\lambda}_0)\,\tilde{\mathbf{i}}_s - \mathbf{i}_{s0}\tilde{R}_s - \mathbf{J}\boldsymbol{\psi}_{s0}\omega_\varepsilon\end{aligned} \tag{23}$$

Based on this equation, approximate open-loop amplifications from the parameter errors to $\tilde{i}_d$ and ω_ε are considered, and the adaptation gains are related to the corresponding bandwidths.

1) PM Flux Adaptation: At medium and high speeds, the system (23) can be approximated as

$$\tilde{\mathbf{i}}_s = -\mathbf{L}^{-1}\,(\mathbf{J}\boldsymbol{\psi}_{s0} - \mathbf{L}\mathbf{J}\mathbf{i}_{s0})\,\tilde{\theta}_m - \mathbf{L}^{-1}\begin{bmatrix}\tilde{\psi}_{pm}\\ 0\end{bmatrix} \tag{24}$$

or in the component form

$$\tilde{i}_d = -\frac{(L_d - L_q)i_{q0}}{L_d}\tilde{\theta}_m - \frac{1}{L_d}\tilde{\psi}_{pm} \tag{25a}$$

$$\tilde{i}_q = -\frac{\psi_{pm} + (L_d - L_q)i_{d0}}{L_q}\tilde{\theta}_m \tag{25b}$$

Since $\tilde{i}_q$ provides information on $\tilde{\theta}_m$, it is used for speed adaptation according to (8).[2] On the other hand, $\tilde{i}_d$ depends strongly on $\tilde{\psi}_{pm}$ (and also depends on $\tilde{\theta}_m$ if $L_d \neq L_q$). After linearization, the PM flux adaptation law (18) is

$$\dot{\tilde{\psi}}_{pm} = \mathbf{k}_{\psi 0}\tilde{\mathbf{i}}_s \tag{26}$$

where the gain may depend on the operating point. Assuming (25a) and (26), the closed-loop system has a bandwidth

$$\alpha_{\psi 0} = k_{\psi 0}/L_d \tag{27}$$

2) Stator Resistance Adaptation: At low speeds, (23) can be approximated as

$$\mathbf{J}\boldsymbol{\psi}_{s0}\omega_\varepsilon = -(R_s\mathbf{I} + \boldsymbol{\lambda}_0)\tilde{\mathbf{i}}_s - \mathbf{i}_{s0}\tilde{R}_s \tag{28}$$

It can be seen that the stator resistance error can be detected only when the motor is loaded. The speed correction term is

$$\omega_\varepsilon = \frac{\boldsymbol{\psi}_{s0}^T\mathbf{J}(R_s\mathbf{I} + \boldsymbol{\lambda}_0)\tilde{\mathbf{i}}_s + \boldsymbol{\psi}_{s0}^T\mathbf{J}\mathbf{i}_{s0}\tilde{R}_s}{||\boldsymbol{\psi}_{s0}||^2} \tag{29}$$

The error component $\tilde{i}_q$ is driven to zero in steady state, and according to (7), the observer gain $\boldsymbol{\lambda}_0$ is small at low speeds. Assuming further that $\boldsymbol{\psi}_{s0} \approx \boldsymbol{\psi}_{pm}$, (29) can be approximated as

$$\omega_\varepsilon \approx -\frac{i_{q0}}{\psi_{pm}}\tilde{R}_s \tag{30}$$

After linearization, the stator resistance adaptation law (19) is

$$\dot{\tilde{R}}_s = k_{R0}\omega_\varepsilon \tag{31}$$

Assuming (30) and (31), the closed-loop system has a bandwidth

$$\alpha_{R0} = i_{q0}k_{R0}/\psi_{pm} \tag{32}$$

which should be positive and can be affected by properly selecting the gain k_{R0} depending on the operating point.

D. Stability Analysis

The local stability of the simultaneous speed and parameter adaptation is analyzed using the linearized open-loop model (22) without the stringent assumptions made in Section IV-C.

1) PM Flux Adaptation: Since the signal injection is not enabled at medium and high speeds, the signal $\omega_\varepsilon = 0$. The linearized system (22) is augmented with the linearized speed adaptation law

$$\dot{\tilde{\omega}}_m = \mathbf{k}_{p0}\dot{\tilde{\mathbf{i}}}_s + \mathbf{k}_{i0}\tilde{\mathbf{i}}_s \tag{33}$$

and the linearized PM flux adaptation law (26). Furthermore, the estimation error of the rotor position is $\dot{\tilde{\theta}}_m = \tilde{\omega}_m$ corresponding to (10). The resulting closed-loop system is given in (38) in the Appendix. The eigenvalues of the closed-loop system were analyzed numerically in different operating points. The parameter values given in Table I were used for the calculations.

As an example, Fig. 5(a) shows eigenvalues obtained with a constant adaptation gain $k_{\psi 0} = 0.2\omega_B L_d$, where ω_B is the base angular speed. The operating-point speed ω_{m0} varies from -1 to 1 p.u., and the operating-point stator current equals the nominal current (corresponding to maximum-torque-per-ampere operating point). Due to symmetry, only the upper half-plane is shown in the pole plot. The vicinity of the origin of Fig. 5(a) is magnified in Fig. 5(b). According to the results, the system is stable above the speed of $\omega_{m0} = 0.05$ p.u. The PM flux and rotor speed adaptation are coupled, but at medium and high speeds, the coupling does not cause problems and the damping of the system is sufficient. If the PM flux adaptation were used at low speeds as well, it would slightly enlarge the unstable region appearing at lowest speeds in the case of salient machines [18].

[2]Assuming (25b) with $L_d = L_q$ and (33), the closed-loop poles of speed and position estimation are placed at $-\alpha_{fo}$ if the gains in (9) are used.

TABLE I
MOTOR DATA

Nominal power	2.2 kW
Nominal voltage U_N	370 V
Nominal current I_N	4.3 A
Nominal frequency f_N	75 Hz
Nominal speed	1 500 r/min
Nominal torque T_N	14.0 Nm
Number of pole pairs p	3
Stator resistance R_s	3.59 Ω
Direct-axis inductance L_d	36.0 mH
Quadrature-axis inductance L_q	51.0 mH
PM flux ψ_{pm}	0.545 Vs
Total moment of inertia	0.015 kgm^2

2) Stator Resistance Adaptation: The signal injection is used at low speeds while the PM flux adaptation is disabled. The system (22) is augmented with the linearized speed-adaptation law (33) and the linearized resistance adaptation law (31). Furthermore, the PI mechanism (15) is linearized as

$$\dot{\omega}_\varepsilon = 2K_{\varepsilon 0}(\gamma_{p0}\dot{\tilde{\theta}}_m + \gamma_{i0}\tilde{\theta}_m) \tag{34}$$

where $\varepsilon = 2K_{\varepsilon 0}\tilde{\theta}_m$ is assumed corresponding to (13). The resulting closed-loop system is given in (39) in the Appendix.

Fig. 5(c) shows dominating eigenvalues as the operating-point speed ω_{m0} varies from $-\omega_\Delta$ to ω_Δ and the operating-point stator current equals the nominal current (corresponding to maximum-torque-per-ampere operating point). The bandwidth α_{i0} of the signal injection mechanism approaches zero when $|\omega_{m0}|$ approaches ω_Δ according to (17). Therefore, the two eigenvalues in Fig. 5(c) move towards the origin, and the order of the system decreases from six to four at $|\omega_{m0}| = \omega_\Delta$. All the eigenvalues are located in the left half-plane, and the system is stable.

E. Gain Scheduling

The adaptation of the stator resistance is in use only at low speeds where the HF signal injection method is used. The PM flux adaptation is not used simultaneously with the stator resistance adaptation, and is enabled when the rotor speed is higher than ω_Δ.

The gain k_ψ for the PM flux adaptation is varied according to

$$k_\psi = k'_\psi g(\hat{\omega}_m) \tag{35}$$

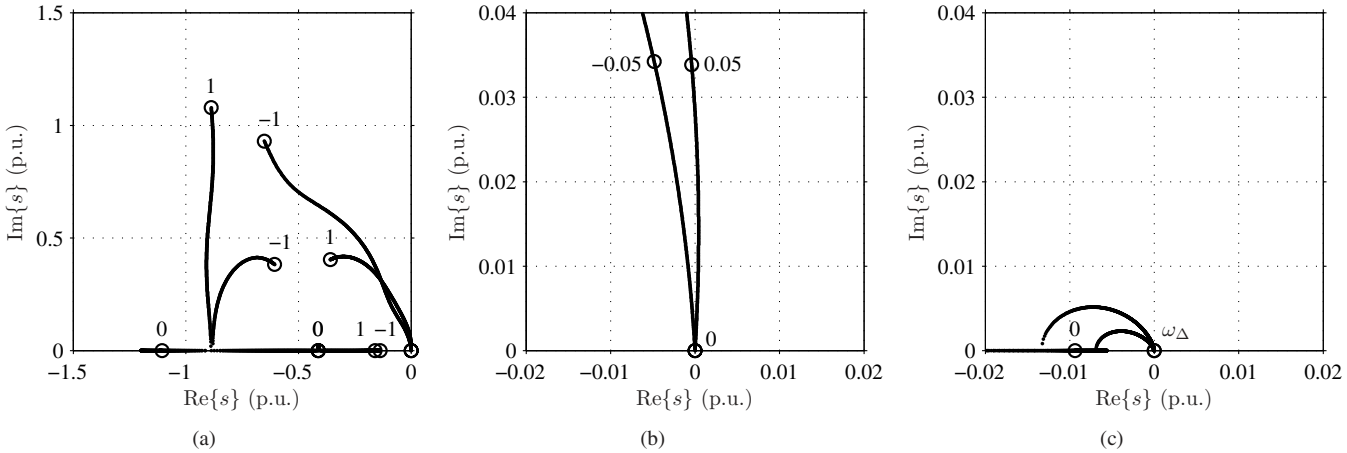

Fig. 5. Eigenvalues of the closed-loop system as ω_{m0} is varied: (a) simultaneous speed and PM flux estimation; (b) the vicinity of the origin of (a) is magnified; (c) simultaneous speed and stator resistance estimation with HF signal injection.

where k'_ψ is a positive constant and $g(\hat{\omega}_m)$ is the speed-dependent function shown in Fig. 3. At speeds higher than ω_ψ, the gain k_ψ is thus kept constant.

In order to have a nonnegative bandwidth (32) for the stator resistance adaptation, the gain k_R and the current i_q must have the same sign. A constant bandwidth α_R is not feasible, since $i_q = 0$ would imply infinite adaptation gain. A signum function in the gain k_R could cause chattering near zero i_q. Therefore, the gain k_R is changed proportionally to i_q, i.e.

$$k_R = \alpha'_R f(\hat{\omega}_m)\hat{\psi}_{pm} i_q / I_B^2 \tag{36}$$

The parameter α'_R is a constant corresponding to the adaptation bandwidth at zero speed and at approximately nominal load, I_B is the base value of the current, and $f(\hat{\omega}_m)$ is the speed-dependent function shown in Fig. 3.

V. Results

The proposed method was investigated by means of simulations and laboratory experiments. The MATLAB/Simulink environment was used for the simulations. The data of the six-pole interior-magnet PMSM (2.2 kW, 1500 rpm) are given in Table I. The base values for voltage, current, and angular speed are defined as $U_B = \sqrt{2/3}U_N$, $I_B = \sqrt{2}I_N$, and $\omega_B = 2\pi f_N$, respectively.

Constant d- and q-axis inductances were used for the simulations. The PMSM used in the laboratory experiments has a laminated rotor with buried permanent magnets. The measured inductances of this motor type decrease with the frequency, but the inductance variations are small at frequencies below 1–2 kHz [23]. The influence of magnetic saturation on the experimental PMSM is negligible even if 150% of the nominal current is applied to the machine.

The electromagnetic torque is limited to 22 Nm, which is 1.57 times the nominal torque T_N. The nominal dc-link voltage is 540 V, and the switching frequency and the sampling frequency are both 5 kHz. The high-frequency carrier excitation signal has a frequency of 833 Hz and a maximum amplitude of $\hat{u}'_c = 40$ V, resulting in a maximum HF current amplitude of 0.22 A or 0.04 p.u. The HF carrier excitation signal is synchronized to the sampling, the sampling frequency being six times the excitation frequency. The transition speeds are $\omega_\Delta = 0.13$ p.u. and $\omega_\psi = 0.2$ p.u., the resistance adaptation bandwidth $\alpha'_R = 0.01$ p.u., and the constant $k'_\psi = 0.2\omega_B L_d$. The current and speed control bandwidths are 5.33 p.u. and 0.067 p.u., respectively, the speed adaptation bandwidth $\alpha_{fo} = 0.667$ p.u., and the bandwidth of the PI mechanism $\alpha'_i = 0.067$ p.u.

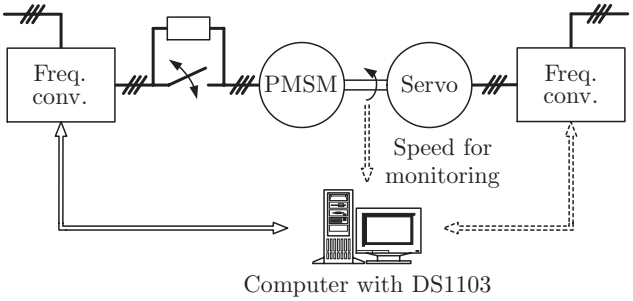

Fig. 6. Experimental setup. Mechanical load is provided by a servo drive.

The experimental setup is illustrated in Fig. 6. The PMSM is fed by a frequency converter that is controlled by a dSPACE DS1103 PPC/DSP board. Mechanical load is provided by a PMSM servo drive. An incremental encoder is used for monitoring the actual rotor speed and position. The dc-link voltage of the converter is measured, and a simple current feedforward compensation for dead times and power device voltage drops is applied [24].

In the experiments, the estimates of the stator resistance and the PM flux were compared with their actual values. The actual stator resistance was identified by measuring the dc resistances of the winding phases, and the PM flux was identified by means of an open-loop back-emf measurement. The temperature of the motor was approximately constant during the experiments. Because the actual parameters are not known precisely, simulations were carried out in addition to the experiments for investigating the convergence of the parameter adaptation.

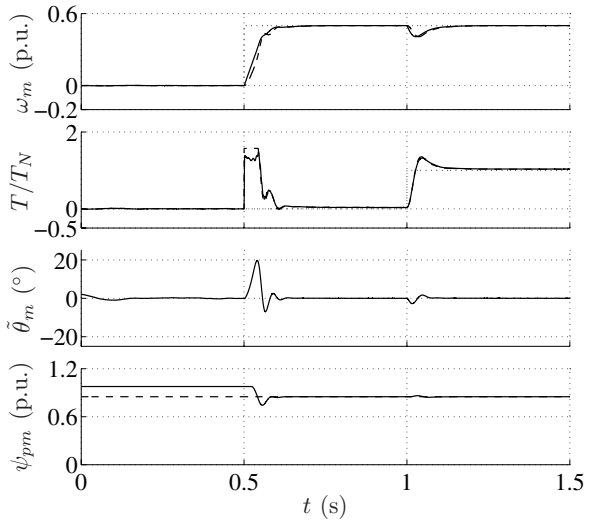

Fig. 7. Simulation results showing PM flux adaptation. First subplot shows electrical angular speed of the rotor (solid), its estimate (dashed), and its reference (dotted). Second subplot shows the load torque reference (dotted), the electromagnetic torque (solid), and its estimate (dashed). Third subplot shows the estimation error of the rotor position. Last subplot shows the PM flux (dashed) and its estimate (solid).

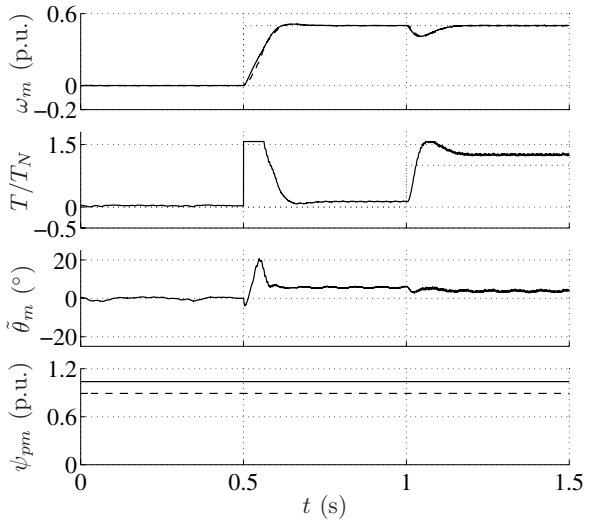

(a)

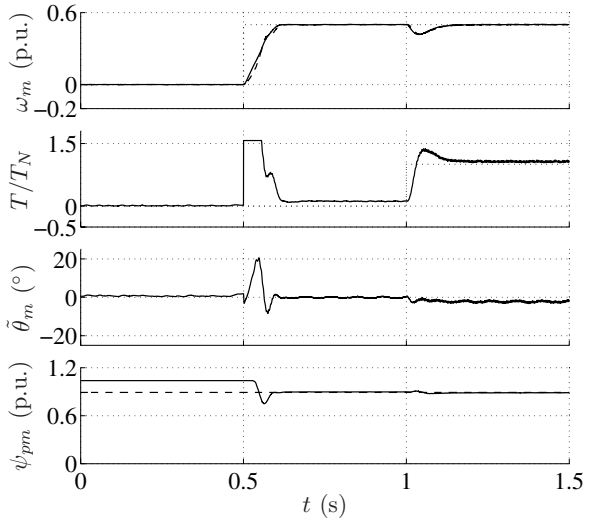

(b)

Fig. 8. Experimental results showing PM flux adaptation: (a) without parameter adaptation; (b) with parameter adaptation. First subplot shows the electrical angular speed of the rotor (solid), its estimate (dashed), and its reference (dotted). Second subplot shows the load torque reference (dashed) and the electromagnetic torque estimate (solid). Third subplot shows the estimation error of the rotor position. Last subplot shows the PM flux (dashed) and its estimate (solid).

A. PM Flux Adaptation

Simulation results showing the behavior of the estimated PM flux are depicted in Fig. 7. The estimated flux is 15% larger than its actual value in the beginning of the simulations, and other parameter estimates are equal to the actual values in the motor model. The speed reference is changed from zero to 0.5 p.u. at $t = 0.5$ s, and a nominal load torque step is applied at $t = 1$ s. After the acceleration at $t = 0.5$ s, the PM flux error is practically removed, and the load torque does not affect the PM flux adaptation.

The effect of the PM flux adaptation on the performance of the drive was investigated experimentally. Fig. 8 shows results corresponding to the simulation in Fig. 7, and Fig. 9 shows results in constant-speed operation. In Fig. 8(a), the parameter adaptation is not in use, whereas in Fig. 8(b), the adaptation is used. Fig. 8(a) shows that the inaccurate PM flux estimate causes an error in the rotor position estimate both at no load and when a load torque is applied. In addition, the electromagnetic torque is lower than the estimated torque. According to Fig. 8(b), the adaptation practically removes the PM flux error in less than 0.2 s after the motor is started, and the errors in the rotor position and the torque are reduced.

In Fig. 9, the rotor speed is 0.5 p.u. and the load torque is at the positive nominal value. The PM flux estimate is forced to an erroneous value at $t \approx 0.6$ s, and the adaptation is enabled again at $t \approx 1$ s. The inaccurate PM flux estimate causes an error in the electromagnetic torque estimate, and the position estimation error also impairs the performance of the drive. After $t \approx 1$ s, the estimated PM flux converges close to its actual value quickly, leading to a reduced position estimation error and improved torque estimation accuracy.

B. Stator Resistance Adaptation

Fig. 10 shows simulation results obtained at zero speed reference. Except the stator resistance, the parameter values used in the controller were equal to those of the motor model. In the beginning of the simulation, the stator resistance estimate is 15% smaller than the actual stator resistance. A nominal load torque step is applied at $t = 1$ s, and the signal injection method corrects the resulting position estimation error through the signal ω_ε. When ω_ε increases, the stator resistance estimate starts converging to the actual resistance immediately. At $t = 2$ s, a 1-Ω step increase (corresponding to 28%) occurs in the stator resistance. The signal injection again detects the resulting position error, and the estimated resistance follows the actual stator resistance. The stator resistance estimate converges close to the actual resistance in less than 1 s.

Experimental results obtained in low-speed operation are depicted in Figs. 11 and 12, showing the behavior of the

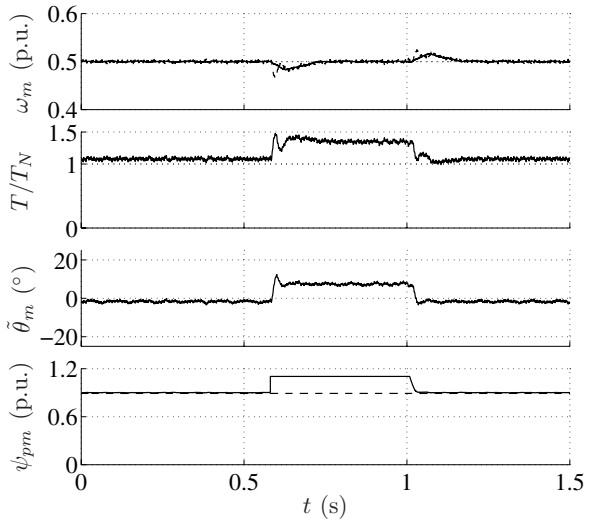

Fig. 9. Experimental results showing PM flux adaptation. PM flux estimate is forced to erroneous value at $t \approx 0.6$ s, and adaptation is enabled again at $t \approx 1$ s. Explanations of the curves are as in Fig. 8.

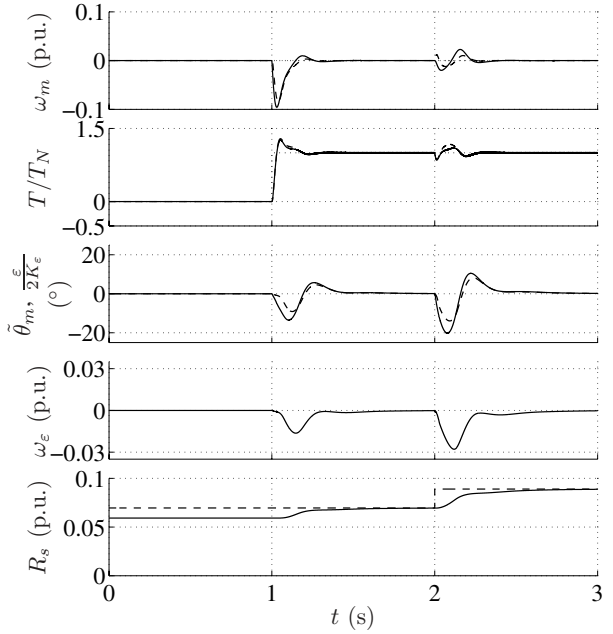

Fig. 10. Simulation results showing stator resistance adaptation. First subplot shows electrical angular speed of the rotor (solid), its estimate (dashed), and its reference (dotted). Second subplot shows the load torque reference (dotted), the electromagnetic torque (solid), and its estimate (dashed). Third subplot shows the estimation error of the rotor position (solid) and the error signal of the signal injection method scaled to the same amplitude with the position estimation error (dashed). Fourth subplot shows the signal ω_ε. Last subplot shows the stator resistance (dashed) and its estimate (solid).

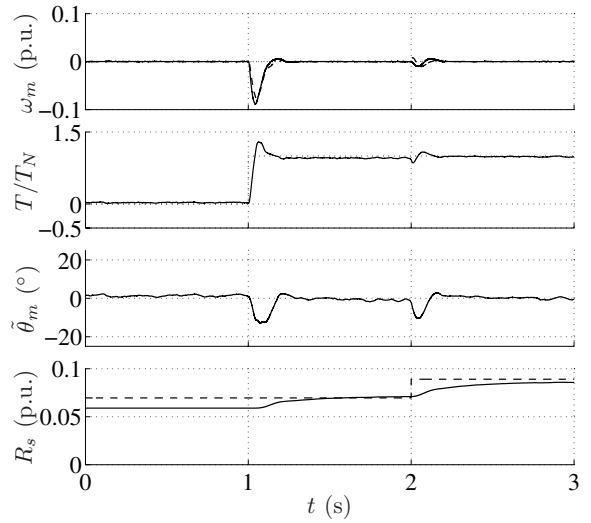

Fig. 11. Experimental results showing stator resistance adaptation. First subplot shows the electrical angular speed of the rotor (solid), its estimate (dashed), and its reference (dotted). Second subplot shows the load torque reference (dashed) and the electromagnetic torque estimate (solid). Third subplot shows the estimation error of the rotor position. Last sublot shows the stator resistance (dashed) and its estimate (solid).

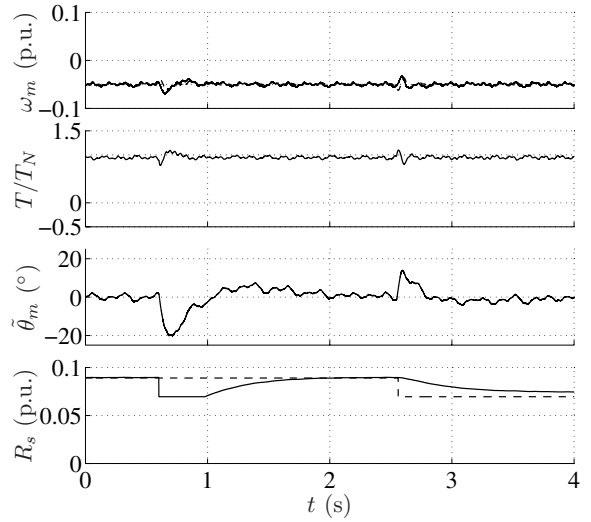

Fig. 12. Experimental results showing stator resistance adaptation. Stator resistance estimate is forced to incorrect value at $t \approx 0.6$ s, and adaptation is activated again at $t \approx 1$ s. Explanations of the curves are as in Fig. 11.

stator resistance adaptation. Additional 1-Ω resistors were added between the frequency converter and the PMSM as shown in Fig. 6. The resistance was changed stepwise by opening or closing a manually-operated three-phase switch connected in parallel with the resistors. The experiment in Fig. 11 corresponds to the simulation in Fig. 10. The error in the stator resistance estimate is decreased after the load torque step at $t = 1$ s, and the estimated stator resistance follows the actual resistance after the stepwise increase at $t = 2$ s. In the experiment of Fig. 12, the drive is operating at very low speed ($\omega_m = -0.05$ p.u.) in the regenerating mode. The load torque is at the positive nominal value. The stator resistance estimate is forced to an incorrect value at $t \approx 0.6$ s. When the resistance adaptation is activated again at $t \approx 1$ s, the estimated resistance returns close to the actual resistance in about 1 second. After the stepwise decrease in the resistance at $t \approx 2.5$ s, the estimated resistance settles close to the new value.

The effect of the stator resistance adaptation on the overall performance of the drive was investigated by means of the experiment of Fig. 13. The stator resistance estimate is initially 15% greater than the actual resistance, and the speed reference is zero. A nominal load torque step is applied at $t = 1$ s, and an acceleration to $\omega_m = 0.15$ p.u. occurs at $t = 2$ s. In Fig. 13(a), the parameter adaptation is not in use, whereas in

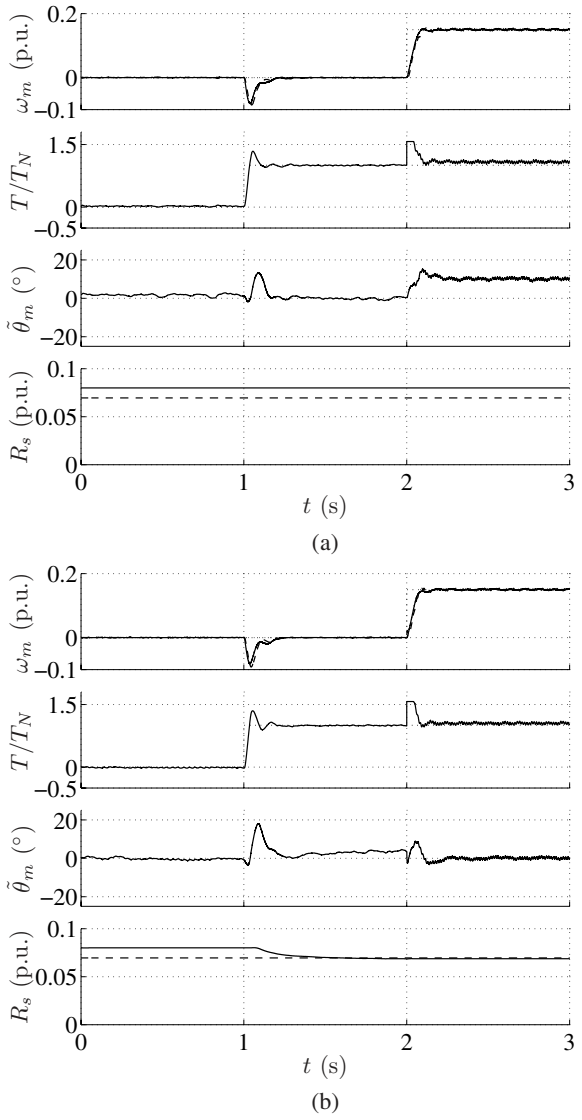

Fig. 13. Experimental results showing stator resistance adaptation: (a) without parameter adaptation; (b) with parameter adaptation. Explanations of the curves are as in Fig. 11.

Fig. 13(b), the adaptation is used. In both cases, the signal injection corrects the position estimation error at zero speed. However, when the stator resistance adaptation is not in use, the removal of the signal ω_ε as the speed increases above ω_Δ leads to a position estimation error. When the stator resistance adaptation is in use, the stator resistance estimate converges close to its actual value, and the position estimation error after the acceleration at $t = 2$ s is reduced. It was found that with a 28% error in the resistance, the drive becomes unstable without the stator resistance adaptation. Hence, the stator resistance adaptation improves the performance significantly and even ensures stable operation. It is to be noted that in the experiments in Figs. 11 to 13, the inverter unidealities contribute to the resistance seen by the controller. Therefore, the estimated resistance is not precisely equal to the actual resistance, but it takes into account the resistive voltage drops in the power devices.

VI. Conclusions

This paper proposed a method for the estimation of the stator resistance and the PM flux in a sensorless PMSM drive. The adaptive observer augmented with an HF signal injection technique at low speeds was used for the adaptation of the parameters in addition to the speed and position estimation. The tuning of the adaptation gains and the local stability of the system were investigated by means of small-signal analysis. The simulation and experimental results show that the stator resistance adaptation reduces the resistance error significantly. The high-frequency signal injection removes the position estimation error in steady state even without any resistance adaptation, but the good accuracy of the resistance estimate is essential when the signal injection is not in use. The PM flux adaptation reduces the position estimation error at medium and high speeds and improves the electromagnetic torque estimation accuracy. The parameter estimates converge rapidly close to the actual parameters, and the sensitivity to the parameter variations is reduced. Since both the stator resistance and the PM flux depend on the temperature, it could be possible to estimate the temperature based on the parameter being adapted, and the temperature information could be used for updating the parameter not being adapted. This kind of simultaneous adaptation of both parameters is a suitable topic for future research.

Appendix
Linearized Closed-Loop Systems

The system (22) is expressed as a state-space representation in (37). The linearized closed-loop system corresponding to the simultaneous speed and PM flux adaptation is given in (38). It is to be noted that the terms $\mathbf{k}_{p0}\mathbf{d}_\psi$ and $\mathbf{k}_{i0}\mathbf{d}_\psi$ vanish due to the speed adaptation gains used in (8). Therefore, those terms have been omitted in (38). When $\tilde{\psi}_{pm} = 0$ is assumed, the linearized model (38) reduces to the model presented in [18]. The linearized closed-loop system corresponding to the speed and stator resistance adaptation is given in (39). The local stability of the proposed system depends on the eigenvalues of the state matrices in (38) and (39).

Acknowledgement

The authors would like to thank the reviewers for their professional work and helpful suggestions.

References

[1] R. Wu and G. R. Slemon, "A permanent magnet motor drive without a shaft sensor," *IEEE Trans. Ind. Applicat.*, vol. 27, no. 5, pp. 1005–1011, Sept./Oct. 1991.

[2] R. B. Sepe and J. H. Lang, "Real-time observer-based (adaptive) control of a permanent-magnet synchronous motor without mechanical sensors," *IEEE Trans. Ind. Applicat.*, vol. 28, no. 6, pp. 1345–1352, Nov./Dec 1992.

[3] M. Schroedl, "Sensorless control of AC machines at low speed and standstill based on the INFORM method," in *Conf. Rec. IEEE-IAS Annu. Meeting*, vol. 1, San Diego, CA, Oct. 1996, pp. 270–277.

[4] P. L. Jansen and R. D. Lorenz, "Transducerless position and velocity estimation in induction and salient AC machines," *IEEE Trans. Ind. Applicat.*, vol. 31, no. 2, pp. 240–247, March/April 1995.

$$\dot{\tilde{\boldsymbol{\psi}}}_s = \underbrace{-(R_s\mathbf{I}+\boldsymbol{\lambda}_0+\omega_{m0}\mathbf{JL})\mathbf{L}^{-1}}_{\mathbf{A}}\tilde{\boldsymbol{\psi}}_s + \underbrace{(R_s\mathbf{I}+\boldsymbol{\lambda}_0)\mathbf{L}^{-1}\left(\mathbf{J}\boldsymbol{\psi}_{s0}-\mathbf{LJi}_{s0}\right)}_{\mathbf{b}_\theta}\tilde{\theta}_m + \underbrace{(R_s\mathbf{I}+\boldsymbol{\lambda}_0)\mathbf{L}^{-1}\begin{bmatrix}1\\0\end{bmatrix}}_{\mathbf{b}_\psi}\tilde{\psi}_{pm} \underbrace{-\mathbf{i}_{s0}}_{\mathbf{b}_R}\tilde{R}_s \underbrace{-\mathbf{J}\boldsymbol{\psi}_{s0}}_{\mathbf{b}_\varepsilon}\omega_\varepsilon \tag{37a}$$

$$\tilde{\mathbf{i}}_s = \underbrace{\mathbf{L}^{-1}}_{\mathbf{C}}\tilde{\boldsymbol{\psi}}_s \underbrace{-\mathbf{L}^{-1}\left(\mathbf{J}\boldsymbol{\psi}_{s0}-\mathbf{LJi}_{s0}\right)}_{\mathbf{d}_\theta}\tilde{\theta}_m \underbrace{-\mathbf{L}^{-1}\begin{bmatrix}1\\0\end{bmatrix}}_{\mathbf{d}_\psi}\tilde{\psi}_{pm} \tag{37b}$$

$$\begin{bmatrix}\dot{\tilde{\boldsymbol{\psi}}}_s\\ \dot{\tilde{\theta}}_m\\ \dot{\tilde{\omega}}_m\\ \dot{\tilde{\psi}}_{pm}\end{bmatrix} = \begin{bmatrix}\mathbf{A} & \mathbf{b}_\theta & \mathbf{0} & \mathbf{b}_\psi\\ \mathbf{0} & 0 & 1 & 0\\ \mathbf{k}_{p0}\mathbf{CA}+\mathbf{k}_{i0}\mathbf{C} & \mathbf{k}_{p0}\mathbf{Cb}_\theta+\mathbf{k}_{i0}\mathbf{d}_\theta & \mathbf{k}_{p0}\mathbf{d}_\theta & \mathbf{k}_{p0}\mathbf{Cb}_\psi\\ \mathbf{k}_{\psi0}\mathbf{C} & \mathbf{k}_{\psi0}\mathbf{d}_\theta & 0 & \mathbf{k}_{\psi0}\mathbf{d}_\psi\end{bmatrix}\begin{bmatrix}\tilde{\boldsymbol{\psi}}_s\\ \tilde{\theta}_m\\ \tilde{\omega}_m\\ \tilde{\psi}_{pm}\end{bmatrix} \tag{38}$$

$$\begin{bmatrix}\dot{\tilde{\boldsymbol{\psi}}}_s\\ \dot{\tilde{\theta}}_m\\ \dot{\tilde{\omega}}_m\\ \dot{\omega}_\varepsilon\\ \dot{\tilde{R}}_s\end{bmatrix} = \begin{bmatrix}\mathbf{A} & \mathbf{b}_\theta & \mathbf{0} & \mathbf{b}_\varepsilon & \mathbf{b}_R\\ \mathbf{0} & 0 & 1 & 0 & 0\\ \mathbf{k}_{p0}\mathbf{CA}+\mathbf{k}_{i0}\mathbf{C} & \mathbf{k}_{p0}\mathbf{Cb}_\theta+\mathbf{k}_{i0}\mathbf{d}_\theta & \mathbf{k}_{p0}\mathbf{d}_\theta & \mathbf{k}_{p0}\mathbf{Cb}_\varepsilon & \mathbf{k}_{p0}\mathbf{Cb}_R\\ \mathbf{0} & 2K_{\varepsilon0}\gamma_{i0} & 2K_{\varepsilon0}\gamma_{p0} & 0 & 0\\ \mathbf{0} & 0 & 0 & k_{R0} & 0\end{bmatrix}\begin{bmatrix}\tilde{\boldsymbol{\psi}}_s\\ \tilde{\theta}_m\\ \tilde{\omega}_m\\ \omega_\varepsilon\\ \tilde{R}_s\end{bmatrix} \tag{39}$$

[5] M. Tursini, R. Petrella, and F. Parasiliti, "Sensorless control of an IPM synchronous motor for city-scooter applications," in *Conf. Rec. IEEE-IAS Annu. Meeting*, vol. 3, Salt Lake City, UT, Oct. 2003, pp. 1472–1479.

[6] A. Piippo, M. Hinkkanen, and J. Luomi, "Sensorless control of PMSM drives using a combination of voltage model and HF signal injection," in *Conf. Rec. IEEE-IAS Annu. Meeting*, vol. 2, Seattle, WA, Oct. 2004, pp. 964–970.

[7] K.-H. Kim, S.-K. Chung, G.-W. Moon, I.-C. Baik, and M.-J. Youn, "Parameter estimation and control for permanent magnet synchronous motor drive using model reference adaptive technique," in *Proc. IEEE IECON'95*, vol. 1, Orlando, FL, Nov. 1995, pp. 387–392.

[8] T. Sebastian, "Temperature effects on torque production and efficiency of PM motors using NdFeB magnets," *IEEE Trans. Ind. Applicat.*, vol. 31, no. 2, pp. 353–357, Mar./Apr. 1995.

[9] R. Krishnan and P. Vijayraghavan, "Fast estimation and compensation of rotor flux linkage in permanent magnet synchronous machines," in *Proc. IEEE ISIE'99*, vol. 2, Bled, Slovenia, July 1999, pp. 661–666.

[10] X. Xi, Z. Meng, L. Yongdong, and L. Min, "On-line estimation of permanent magnet flux linkage ripple for PMSM based on a kalman filter," in *Proc. IEEE IECON'06*, Paris, France, Nov. 2006, pp. 1171–1175.

[11] M. Elbuluk, L. Tong, and I. Husain, "Neural-network-based model reference adaptive systems for high-performance motor drives and motion controls," *IEEE Trans. Ind. Applicat.*, vol. 38, no. 3, pp. 879–886, May/June 2002.

[12] P. Niazi and H. Toliyat, "On-line parameter estimation of permanent magnet assisted synchronous reluctance motor drives," in *Proc. IEEE IEMDC'05*, San Antonio, TX, May 2005, pp. 1031–1036.

[13] S. Wilson, G. Jewell, and P. Stewart, "Resistance estimation for temperature determination in PMSMs through signal injection," in *Proc. IEEE IEMDC'05*, San Antonio, TX, May 2005, pp. 735–740.

[14] F. Briz, M. W. Degner, J. M. Guerrero, and A. B. Diez, "Temperature estimation in inverter fed machines using high frequency carrier injection," in *Conf. Rec. IEEE-IAS Annu. Meeting*, New Orleans, LA, Sept. 2007, pp. 2030–2037.

[15] M. Eskola and H. Tuusa, "Comparison of MRAS and novel simple method for position estimation in PMSM drives," in *Proc. IEEE PESC'03*, vol. 2, Acapulco, Mexico, June 2003, pp. 550– 555.

[16] K.-W. Lee, D.-H. Jung, and I.-J. Ha, "An online identification method for both stator resistance and back-emf coefficient of PMSMs without rotational transducers," *IEEE Trans. Ind. Electron.*, vol. 51, no. 2, pp. 507–510, Apr. 2004.

[17] S. Ichikawa, M. Tomita, S. Doki, and S. Okuma, "Sensorless control of permanent-magnet synchronous motors using online parameter identification based on system identification theory," *IEEE Trans. Ind. Electron.*, vol. 53, no. 2, pp. 363–372, Apr. 2006.

[18] A. Piippo, M. Hinkkanen, and J. Luomi, "Analysis of an adaptive observer for sensorless control of interior permanent magnet synchronous motors," *IEEE Trans. Ind. Electron.*, vol. 55, no. 2, Feb. 2008.

[19] T. Jahns, G. Kliman, and T. Neumann, "Interior permanent-magnet synchronous motors for adjustable-speed drives," *IEEE Trans. Ind. Applicat.*, vol. 22, no. 4, pp. 738–747, July/Aug. 1986.

[20] L. Harnefors and H.-P. Nee, "A general algorithm for speed and position estimation of AC motors," *IEEE Trans. Ind. Electron.*, vol. 47, no. 1, pp. 77–83, Feb. 2000.

[21] M. Saejia and S. Sangwongwanich, "Averaging analysis approach for stability analysis of speed-sensorless induction motor drives with stator resistance estimation," *IEEE Trans. Ind. Electron.*, vol. 53, no. 1, pp. 162–177, Feb. 2006.

[22] M. Rashed, P. F. A. MacConnell, and A. F. Stronach, "Nonlinear adaptive state-feedback speed control of a voltage-fed induction motor with varying parameters," *IEEE Trans. Ind. Applicat.*, vol. 42, no. 3, pp. 723–732, May/June 2006.

[23] S. Øvrebø, "Sensorless control of permanent magnet synchronous machines," Doct. thesis, Norwegian University of Science and Technology, 2004.

[24] J. K. Pedersen, F. Blaabjerg, J. W. Jensen, and P. Thogersen, "An ideal PWM-VSI inverter with feedforward and feedback compensation," in *Proc. EPE'93*, vol. 5, Brighton, UK, Sept. 1993, pp. 501–507.

AUTHORS' BIOGRAPHIES

Antti Piippo is a Design Engineer at ABB Oy, Helsinki, Finland. In 2003, he joined Helsinki University of Technology, where he worked as a research scientist at the Power Electronics Laboratory until 2007. His current research interests include the control of synchronous motor drives. He received the M.Sc. (Eng.) degree from Helsinki University of Technology in 2003.

Marko Hinkkanen (M'06) is currently an Acting Professor in the Department of Electrical and Communications Engineering, Helsinki University of Technology, Espoo, Finland. Since 2000, he has been with the Power Electronics Laboratory, Helsinki University of Technology. His research interests are in the areas of electric drives and electric machines. He received the M.Sc.(Eng.) and D.Sc.(Tech.) degrees from Helsinki University of Technology, in 2000 and 2004, respectively.

Jorma Luomi (M'92) is a Professor in the Department of Electrical Engineering, Helsinki University of Technology, Espoo, Finland. He joined Helsinki University of Technology in 1980, and from 1991 to 1998 he was a Professor at Chalmers University of Technology. His research interests are in the areas of electric drives, electric machines, and numerical analysis of electromagnetic fields. He received the M.Sc.(Eng.) and D.Sc.(Tech.) degrees from Helsinki University of Technology, in 1977 and 1984, respectively.